Table of Contents

Edited	Approved
Specialist Committee on Detailed Flow Measurement Techniques of the 27th ITTC	27th ITTC 2014
Date 03/2014	Date 09/2014

Uncertainty Analysis for Particle Image Velocimetry Using a System-Level Approach

1. PURPOSE OF GUIDELINE

The primary purpose of the current guideline is to outline a method of analysis of the measurement uncertainty for particle image velocimetry (PIV) and stereo PIV (SPIV). Specifically, this guideline will address error sources due to practical issues related to the applications of PIV in hydrodynamic testing facilities, in addition to error sources inherent to the PIV technique itself.

2. SCOPE

Uncertainty in the measurement of a physical quantity can be considered on different levels. The measurement device itself will exhibit an inherent level of measurement error, even in the most ideal condition. In addition, once the measurement device is utilized as part of an experiment, other sources of errors specific to the experimental setup will contribute further to the overall measurement uncertainty. There is a large body of literature dealing with the primary error sources inherent to the PIV technique itself, including calibration error, perspective error, and error due to the determination of correlation peaks between the image pairs. However, errors due to issues associated with the applications of PIV/SPIV in large-scale industrial facilities can contribute significantly to the overall measurement uncertainty. These errors include suboptimal seeding, improper light sheet overlap, large velocity gradients in the interrogation regions and in-plane and out-of-plane loss of particles between the image pairs. In practice, these errors are difficult to estimate due to the fact that they vary widely with each specific application. A rigorous approach is needed in order to achieve estimates of these errors in a realistic test environment. This guideline proposes an approach utilizing a combination of the classical component error estimation and error estimates at the system level, in order to deal comprehensively with the measurement uncertainty of the entire system. The proposed approach is general and applies to two-dimensional two-component PIV (2D2C PIV) as well as stereo-PIV (SPIV).

3. BACKGROUND

Particle image velocimetry is a minimally-invasive quantitative measurement technique suitable for the instantaneous whole-field measurement of spatio-temporal flows. PIV and its variants (stereo-PIV, PTV, etc) have matured considerably over the last decade with many advancements both in the hardware components and in the image-evaluation algorithms. Within the ITTC community, these advancements have led to a broader usage of the technique in a wide range of critical applications.

Uncertainty analysis is an important aspect of any experimental campaign, and this is especially true for PIV measurements. PIV is being increasingly utilized to validate the application of CFD in the design and evaluation of marine vessels and offshore structures; and for such a purpose, it is important to determine the degree of "goodness" of these measurements. Uncertainty analysis for the PIV technique has been a significant focus of the PIV community over the years, but similar to the PIV technique itself, this area remains an evolving field with rapid development still being made.

Over the years, rapid advancements of the PIV technique have been made with the careful consideration of the measurement uncertainty

along the way. For example, Westerweel et al. (1997) utilized both synthetic images of isotropic turbulence and actual measurements of grid-generated turbulence to assess the effect of the window offset technique on the uncertainty of the flow velocity computation. This technique results in a significant increase in the data yield while at the same time optimizing the error in the measurement. By offsetting the interrogation windows according to the mean displacement, the fraction of matched particle images to unmatched particle images is increased, effectively enhancing the signal-to-noise ratio and reducing the uncertainty in the measured particle displacement. Today, most commercial PIV software packages have adopted the multi-pass interrogation schemes with window offset as a standard practice for vector field computation. Prasad et al. (1992) studied the effect of particle image size and concluded that particle image size on the order of one pixel leads to an undesirable effect called pixel locking, but large particle image size (>4 pixels) leads to broadening of the correlation peaks and thus a lower signal-to-noise ratio. Today, it is a commonly accepted practice to tailor the particle size or the pixel resolution so the particle image size is on the order of 2-4 pixels in diameter.

Due to the hard work of these and other investigators, the PIV community today has a good understanding of how to optimize the accuracy of the measurement. We know, for example, that the average particle displacement should be on the order of ¼ of the window size (Keane & Adrian, 1990) and that it is desirable to have around 10 particles within an interrogation window (Keane & Adrian, 1991). We also know that the uncertainty in the measurement can drastically increase with velocity gradient within the interrogation window (Keane & Adrian, 1992). The Detailed Flow Measurement Techniques Committee has compiled these knowledge and "best practices" into a guideline on PIV application in tow tanks and cavitation

tunnels (ITTC 7.5-02-01-04) with the primary goal of assisting the adoption of this measurement technique within the ITTC community.

Even though the consideration of measurement accuracy has been an integral part of advanced PIV developments over the years, analysis of the measurement uncertainty has for the most part been isolated to the specific aspect being investigated and primarily to establish any improvement of a more advanced algorithm over a less advanced one. The assessment of the overall uncertainty of an actual PIV setup in a demanding environment such as tow tanks and cavitation tunnels remain a particular challenge due to the complexity of the system and the many sources of errors that need to be considered for each application. Attempts at estimating component error sources based on the results from the literature usually involve making a fair number of assumptions in order to be relevant to the actual situation. These component errors are then propagated in order to estimate the overall uncertainty. Often time, error sources that are difficult to ascertain are simply ignored altogether.

At first glance, the task of evaluating the overall system performance and uncertainty level of an entire PIV system may indeed appear daunting. It is obvious from the literature that rigorous analyses of even a few error sources can represent a fair level of effort, and many important practical sources of errors have yet to be dealt with in a satisfactory manner. How does one then analyse all or at least most of the important error sources to capture the overall performance and uncertainty of the system in a realistic fashion? A good approach must strike the right balance between scientific rigor and practicality to yield an acceptable estimate of the overall uncertainty without requiring an unrealistic level of effort.

4.   A RANGE OF APPROACH FOR PIV UNCERTAINTY ANALYSIS

As previously observed, one of the most difficult aspects of PIV uncertainty analysis is the fact that each application of PIV is made unique by the particular setup, the flow of interest, and the intended use of the data. As such, the goal of achieving a step-by-step procedure that can be applied to the uncertainty analysis for all applications of PIV appears to be unrealistic. A more pragmatic approach is to recognize that a range of sound and rigorous methodologies can be applied to address various error sources in PIV, with a specific procedure for each application being determined on a case-by-case basis.

The primary goals of the experiment and the intended use of the data play a large part in dictating the appropriate level of detail for the uncertainty analysis. Is the experiment being performed as part of a phenomenology study to obtain a qualitative understanding of the flow? Or is the absolute quantification of the measured data necessary to determine if a set of engineering criteria is met? Is the measurement being used to validate and certify the use of simulation codes for design and evaluation purposes? While it may be adequate to have only a general estimate of the measurement uncertainty for some of these questions, others may demand a more rigorous approach to quantify the error bounds to a higher degree of fidelity.

There are multiple levels of error sources in PIV that need to be considered:

Level 0, error sources inherent to the PIV technique: These errors include calibration error, perspective error, and error due to the determination of correlation peak between the image pairs. These errors exist even in the most ideal conditions but may vary according to specific optical configurations.

Level 1, error sources inherent to the particular setup: These errors include suboptimal seeding, improper light sheet overlap, bending of support struts while underway, etc. These errors arise due to practical issues associated with a complex experimental setup in tow tanks and cavitation tunnels. In practice, the quality of the measurement is largely determined by how well these error sources are managed.

Level 2, error sources inherent to the flow of interest: These errors include large velocity gradients in the interrogation regions and in-plane and out-of-plane loss of particles between the image pairs. These errors arise due to the particular nature of the flow being measured. For example, a complex vortical flow with large out-of-plane motion would exhibit much larger level 2 errors than a low-gradient two-dimensional flow.

There are three broad categories of methodologies that have been used to consider the uncertainty in the measurement for PIV. In addition, some key characteristics of each methodology are noted:

1) Component error estimation approach
   a. Individual error sources are estimated and propagated into an overall uncertainty in the measurement.
   b. The typical method is to estimate the uncertainty level analytically; however, a number of error sources are not easily estimated, preventing the determination of the overall uncertainty level of the entire system.

2) System-level approach using a simulated PIV setup and synthetic images
   a. Individual error sources are not separately determined. Rather a system-level or a sub-system-level determination of the uncertainty level is made using a computer model of

the setup and synthetic images of the particle field.

b. Since the setup is simulated, the fidelity of the computer model needs to be validated. The validation can be performed by comparing the images from the simulation outputs to those from the physical setup.

c. It is possible to analyse flow-based errors due to large velocity magnitude and gradients, including the effects of in-plane and out-of-plane particle loss.

d. It is possible to analyse image-based errors due to sub-optimal seeding density, particle image size, and image pixelization. Attempts can be made to estimate these variables in the actual PIV images and quantify uncertainty level on a vector-by-vector basis.

e. It is possible to utilize this approach in the optimization of the PIV optical setup.

3) System-level approach using the actual physical PIV setup

a. Individual error sources are not separately determined. Rather a system-level or a sub-system-level determination of the uncertainty level is made with the actual PIV setup.

b. Analysis is limited to simple flows, such as uniform flow, as a complex flow in the physical world is not known a priori. For example, the PIV system can be towed through quiescent fluid (with no test model present) and results compared with an assumed uniform flow.

c. This approach can be used with complementary measurements (e.g.

LDV, hotwire, etc) in order to increase the level of confidence of the analysis.

d. Analysis relies on the use of the actual setup, making it impractical in the experimental design stage.

4.1 Component Error Estimation Approach

The traditional manner in which one considers the uncertainty in an experimental measurement is to assume that the desired result is described by a data-reduction equation with a number of dependent variables of the form:

$$r = r(X_1, X_2, \ldots, X_j), \tag{1}$$

and the uncertainty in the result is given by

$$U_r^2 = \left(\frac{\partial r}{\partial X_1}\right)^2 U_{X_1}^2 + \left(\frac{\partial r}{\partial X_2}\right)^2 U_{X_2}^2 + \cdots + \left(\frac{\partial r}{\partial X_j}\right)^2 U_{X_j}^2 . \tag{2}$$

A typical form of the data reduction equation for a PIV measurement of the flow speed u is given by:

$$u = M(\Delta X/\Delta t) + \delta u, \tag{3}$$

where ΔX represents the displacement of the particle images typically based upon the cross-correlation technique, Δt is the time interval between successive images, M is the magnification factor, and δu is additional errors due to particle lag and the projection procedure from the 3-D physical space to the 2-D image plane. Major error sources are identified and estimated that would contribute to the uncertainty in the determination of each dependent variable. These error sources are then combined into the overall uncertainty level of the system using Equation (2).

Even though it is helpful to think of PIV measurements from this conceptual viewpoint, in actual applications, there are many interdependent error sources that are not amenable to be described in such a manner. When one considers the process of implementing a PIV measurement from end to end, as graphically represented in Figure 1, it is clear that the contribution to one error component can come from a number of steps in the process. For example, the error in the determination of ΔX depends on a large number of factors. The experimental setup plays a large role, with the quality of the measurement being dependent on how well the 3-D physical space is imaged onto the 2-D image space, how much of the in-plane velocity is biased by the out-of-plane component, and how well the laser sheet is aligned with the tow direction and the calibration target, etc. The conduct of the experiment also plays a critical part, with the quality of the measurement being dependent on how well the flow is seeded, how long one waits between carriage passes for the turbulence level to subside, and how stiff the support struts are and whether the system bends or vibrates while being towed, etc. Then once the raw images are collected, the process of calculating ΔX itself involves the selection from a range of different correlation schemes and windowing techniques, which could significantly affect the calculated results. Outside of the core PIV vector computation, the manner in which the post-processing schemes are applied to remove outliers and replace them with secondary vectors could affect the results and introduce its own errors.

However, there are a number of error sources which could be effectively analysed by the component estimation approach:

Particle lag

PIV is a flow-field measurement system, based upon the determination of the displacement of tracer particles within the flow, with the fundamental assumption that the particles faithfully follow the flow. In reality, the particles will experience some velocity lag in the presence of flow acceleration when the particle density is different from that of the surrounding fluid. The velocity lag can be estimated from the following equation (Raffel et al., 1998):

$$\Delta u = d_p^2 \frac{(\rho_p - \rho)}{18\mu} a \quad , \qquad (4)$$

where d_p is the particle diameter, and ρ_p is the particle density, and a is the local fluid acceleration. For most water-borne applications, the velocity lag is a small error source.

Timing error

Considering the data reduction equation presented in Equation (3), two sources contribute to the error in Δt: the timing fluctuation from the delay generator and the uncertainty in the pulse timing associated with the laser itself. The total uncertainty in timing can be estimated with using the root sum square of the two sources, and the absolute sensitivity coefficient due to the timing error is given by Equation (5).

$$\frac{\partial u}{\partial (\Delta t)} = -\left(\frac{1}{\Delta t}\right) u \qquad (5)$$

Typically, contribution to the uncertainty in flow velocity from timing is negligible for modern delay generators and pulse lasers.
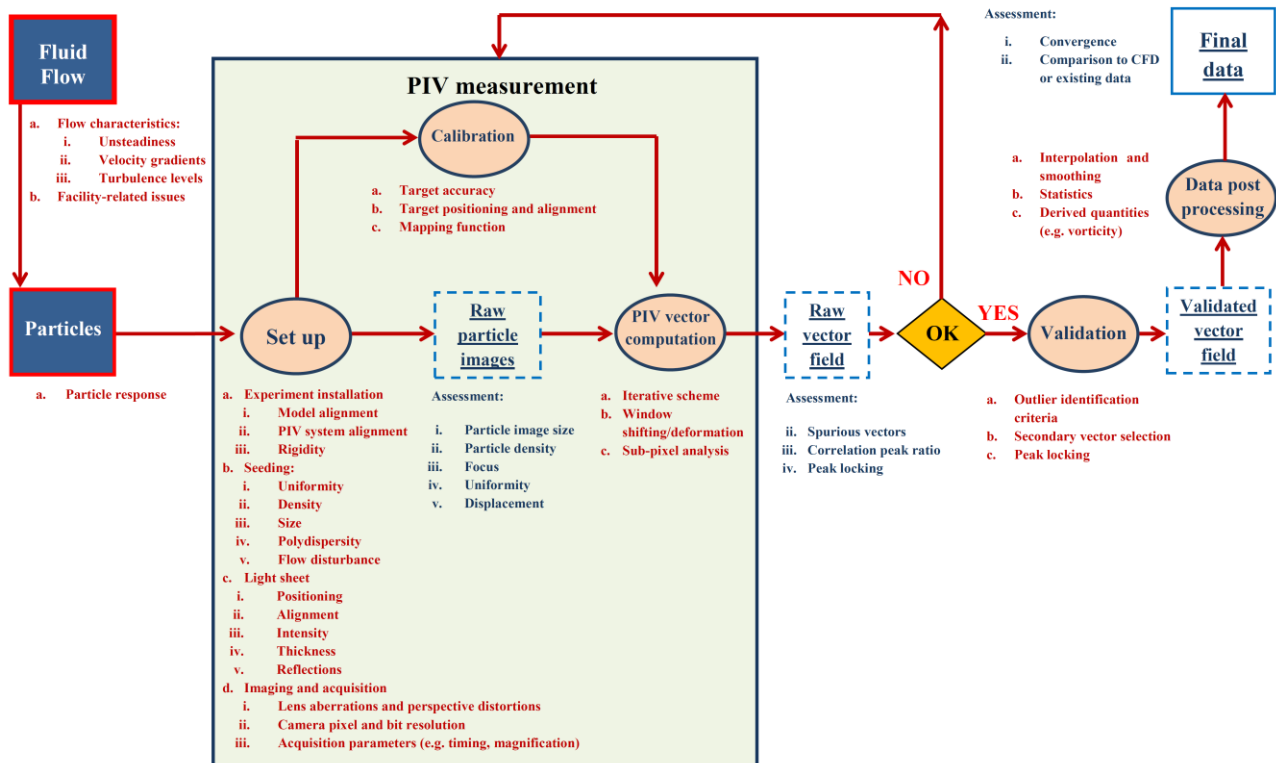
Fig. 1 Flow chart of PIV from the uncertainty analysis viewpoint

Experimental installation and other facility-related Issues

Apart from the errors due to the PIV measurement system, the installation of the experiment and other facility-related issues can ultimately cause the error in the velocity measurement itself. These errors include the misalignment of the model (causing a different flow than the desired one), precision of speed control (leading to error in the reference velocity), and blockage effect or other facility bias (affecting the flow of interest). It is important to estimate the magnitude of these errors and propagate them into the overall uncertainty of the experimental campaign.

4.2 System-Level Approach Using a Simulated PIV Setup and Synthetic Images

An alternative approach that has been used widely to study elemental error sources in PIV involves the use of a simulated PIV system and synthetic images (Westerweel, 1993; Keane & Adrian, 1990, 1991, 1992; Willert, 1996; Stalisnas et al., 2003, 2005, 2008). The first image of the PIV pair is generated by modelling a random distribution of particles within a fluid volume. The flow is assumed to be known, and the second image is generated by advecting the particles from the first image by a displacement equal to the product of the local flow velocity and Δt. The synthetic image pair is used as an input to the PIV algorithm, and the vector field

is calculated and compared to the known solution. In general, the simulations are performed using a simplified simulated PIV setup (simple imaging of a two-dimensional flow with constant magnification and no lens distortion), and simple canonical flows (uniform flow, shear flow, rotational flow, isotropic turbulent flow, etc). Typically, the primary goal is to reach general conclusions on the effects of the parameters of interest and not to evaluate the uncertainty level of a realistic setup. A single parameter is varied at a time, and a large number of simulations are performed to assess the mean and distribution of the results, and the simulations are compared to the known solution for the evaluation of the systematic and random uncertainties. These types of Monte Carlo simulations have been successfully used to study the effects of particle size and density, magnitude of velocity and shear, and the efficacy of various image-evaluation algorithms.

This approach can be extended to assess the overall uncertainty level of a realistic PIV setup. Rather than modelling the system as a simple system to isolate the effect of varying a parameter, the current purpose is to simulate the system as realistically as practical and evaluate the uncertainty level of the system as a whole. The steps that are required are the following:

Selection of a known flow: A range of options is possible, from canonical flows (to determine Level 1 errors) to the flow of interest itself (to determine Level 2 errors). A reasonable way to generate the flow of interest may be to use the solution from a CFD computation on the current problem (if the level of fidelity is adequate). For the purpose of performing the uncertainty analysis, the simulated flow of interest needs only to be representative of the actual physical flow.

Modelling of the particle field: The location in physical space (X, Y, Z), size (d_p), and density of particles within the volume of fluid can be modelled as a uniformly distributed field of particles of a certain size range. The location of each particle is random, and the size may include polydispersity as appropriate.

Modelling of the illumination field: The intensity of the laser illumination can be modelled using varying degrees of realism. The simplest case is uniform intensity. A more realistic model of the laser sheet may have a Gaussian intensity profile in the lateral direction, with exponential decay along beam to simulate attenuation in water. Across sheet, the laser power distribution would be the laser beam profile. In general, the model of the illumination field would return a local illumination intensity as a function of location in three dimensional space: $I_{illum}(X, Y, Z)$. Modelling the illumination field in three-dimensional space is crucial to capture the effect of out-of-plane particle loss.

Modelling of the particle image intensity distribution: A well-established approach is to model the intensity distribution of a particle image using a Gaussian intensity profile (Raffel et al., 1998):

$$I(x, y, z) = I_o exp \left[\frac{-(x-x_o)^2 - (y-y_o)^2}{(1/8)d_\tau^2} \right] \quad (6)$$

where (x, y, z) denotes the position in the image plane. The peak intensity, $I(x, y, z)$, can be modelled as a product of the local illumination intensity and the efficiency factor q, which is a measure of how efficient the incident light is scattered by the particles and imaged onto the sensor:

$$I_o(x, y, z) = q * I_{illum}(X, Y, Z) . \quad (7)$$

The efficiency q is a function of a number of parameters, including particle size, lens aperture, sensitive of the imager, etc. The most practical way to determine q is through a calibration pro-

cess using actual images. The particle image diameter d_τ can be estimated using the following formula (Adrian & Yao, 1985):

$$d_\tau = \sqrt{(Md_p)^2 + d_{diff}^2}\,, \qquad (8)$$

where M is the local magnification factor. d_{diff} is the diffraction-limited minimum image diameter, approximated by the following formula:

$$d_{diff} = 2.44 f_\#(M+1)\lambda\,, \qquad (9)$$

where $f_\#$ is the lens f-number, and λ is the wavelength of the incident light.

Modelling of the imaging system: The model of the imaging system should realistically represent the manner in which the light distribution in the physical space gets imaged onto the image space. For a simple 2D2C system in which the lens axis is perpendicular to the light sheet, it is reasonable to simply use a uniform magnification ratio throughout the entire image: $(x,y) = M*(X,Y)$. The out-of-plane axis is simply ignored.

In the case where the lens axis is not perpendicular to the light sheet or in SPIV applications where the plane of measurement is viewed from a large oblique angle, the situation is more complex. In addition, for underwater applications, another factor which complicates the modelling is the step changes in the indices of refraction as light travels through water and the optical window before it gets imaged by the lens and recorded on the CCD. A simple approach to model a complex imaging system typical in an underwater SPIV setup is presented in Appendix A.

Modelling of the image recording: The model of the image recording primarily involved the pixelization of a continuous distribu-

tion of imaged light onto a discrete light-sensitive sensor array. The continuous light distribution can be piecewise integrated onto the light sensitive portion of each pixel and registered as an integer value in the range of 0 to $2^N - 1$, where N is the number of bits of the camera A/D converter. A more sophisticated image recording model may take into account the fact that for a complex imaging system, a physical plane may get imaged onto a curve, and therefore a portion of the image may be slightly out of focus.

Once the PIV setup has been successfully modelled, it is important to evaluate the quality of the model by comparing the synthetic images with the actual images obtained by the physical setup. Two types of images can be compared: image of a particle field and image of a calibration target. Comparison of the simulated image to the actual image of the calibration target provides the ability to assess the imaging model, and comparison of the particle field images provides additional information on how well the particle size and density are modelled. And by comparing the relative intensity of the particles between the simulated and the actual images, one can accurately quantify the efficiency factor q.

Once the model of the PIV setup is verified to be a good representation of the actual physical setup, the system-level uncertainty analysis of the PIV system can be performed. If one makes the assumptions that the particles faithfully follow the flow or the error due to velocity lag can be quantified and that the errors due to experimental installation or facility issues are small or can be quantified (and propagated later), then a reasonable boundary of the modelled system may be the combination of the "PIV measurement" step (green box as represented in Figure 1) and the "validation" step.

At this point, "setup" in Figure 1 is simulated by steps 3-6; "raw particle images" are modelled

by the synthetic images of the particle field; "calibration" involves the generation of synthetic images of the calibration target and providing these as inputs into calibration module within the actual PIV software package; "PIV vector computation" means exercising the vector computation module within PIV software package to compute the velocity field from the synthetic images; and "validation" means exercising the vector validation module that performs outlier removal and secondary vector replacement within the PIV software package. The flow chart presented in Figure 2 illustrates the system-level approach using a simulated PIV setup from a modelling and software implementation standpoint.

It is possible, using the model of the PIV setup and the actual PIV software package to explore most of the items listed in red in Figure 1. Again, it is important to note that a critical evaluation needs to be performed on a case-by-case basis to determine the appropriate scope of the simulation. For example, if the measurement is performed in a small cavitation tunnel where uniform seeding is readily achieved, one may assume optimal seeding and focus instead on other error sources that may be dominant in the experiment. For tow tank applications, seeding is more difficult and image-based errors due to non-optimal seeding may need to be explored.

4.3 System-Level Approach Using the Actual Physical PIV Setup

Another approach which can be taken to evaluate the uncertainty of the system involves the use of the physical PIV system itself (Willert, 1996). Assuming that a known physical flow can be generated in a reliable fashion, one can perform an actual PIV measurement and compare the results with the assumed-known flow. Typically, in a tow tank, a quiescent flow can be set up by seeding the fluid volume and allowing the turbulence to subside to an acceptable level. The PIV system can then be towed at a known velocity to generate a uniform flow. In a cavitation tunnel, the tunnel can be operated at a steady speed with no model present. This technique represents a good way to baseline the performance of the system in an idealized situation but cannot capture error sources such as those arising from a complex flows and practical issues such as non-optimal seeding. And since the technique relies on the use of the actual physical setup, the approach cannot be used to evaluate the uncertainty level of a conceptual system during the experimental design stage.
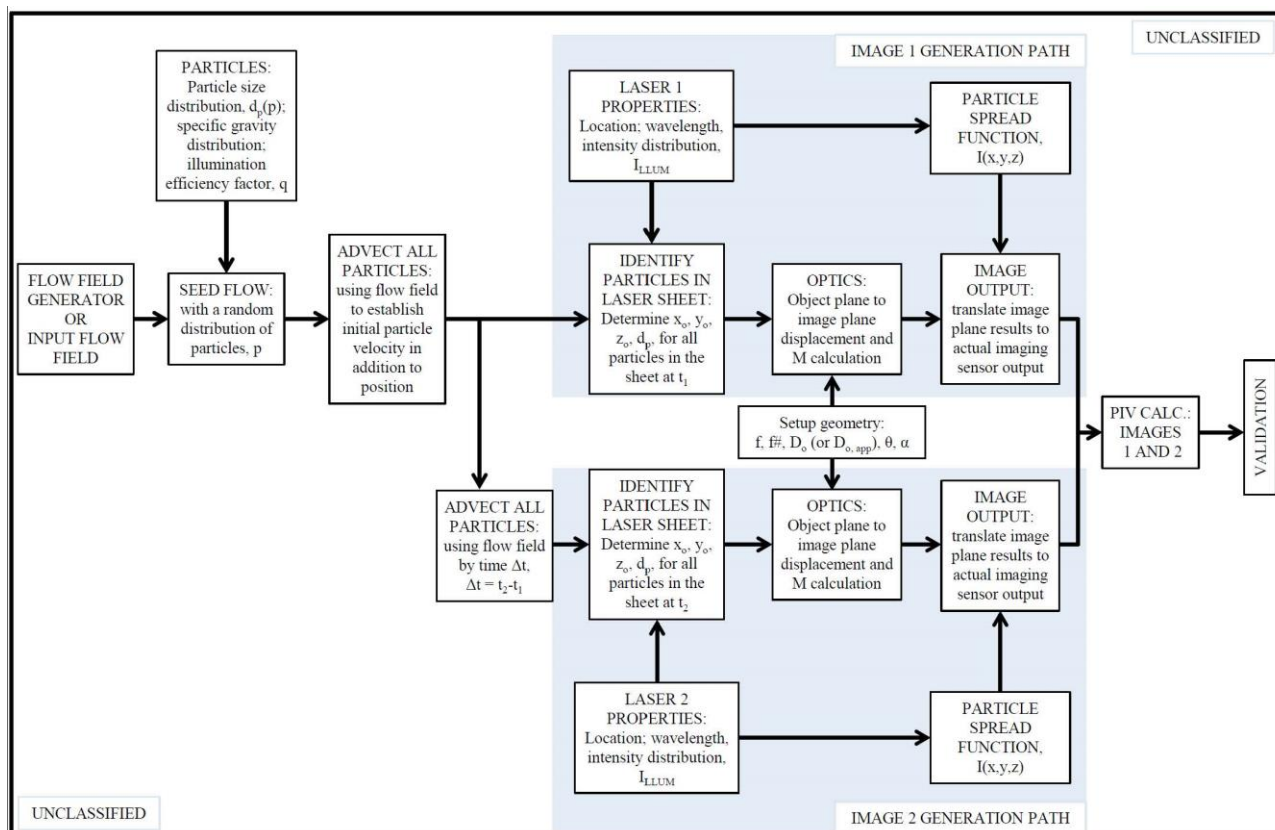
Figure 2: Flow chart illustrating the system-level approach using a simulated PIV setup

5. ASSESSMENT OF THE OVERALL UNCERTAINTY FOR PIV MEASUREMENT

In Section 4, the benefits and drawbacks for the component error estimation approach, the system-level approach using a simulated PIV setup, and the system-level approach using an actual PIV setup are discussed. For each specific application, it is important to determine how these approaches can be effectively used to determine the overall uncertainty of the PIV measurement.

A reasonable approach is the following:

1. Utilize the component error estimation approach as much as possible. In particular, this approach is appropriate for error sources that are distinct from the rest of the system and can be readily estimated analytically. The magnitude of each of the error sources is denoted as $U_{X1}, U_{X2}, U_{X3}, ...$

2. Perform Monte Carlo simulations to evaluate the systematic and random uncertainty of the system using the simulated PIV setup with canonical flows or the flow of interest. The overall uncertainty from this step is denoted as U_{sys}.

3. Repeat step (2) with a simplified flow that can be reliably duplicated with the

physical PIV setup. The overall uncertainty from this step is denoted as U_{sim}.

4. Perform a physical measurement of the simplified flow to determine the baseline uncertainty level of the physical system. The overall uncertainty from this step is denoted as U_{phy}.

5. The difference between U_{sim} and U_{phy} provides a good estimate for the modelling error of the simulated setup, denoted as U_{model}.

6. Propagate the uncertainties estimated with the component error estimation approach with the simulated system-level error and the error due to modelling of the simulated system:

$$U^2 = U_{X1}^2 + U_{X2}^2 + U_{X3}^2 + \cdots + U_{sys}^2 + U_{model}^2 \cdot \tag{10}$$

6. IMPLEMENTING AND VALIDATING THE SYSTEM-LEVEL APPROACH FOR PIV UNCERTAINTY ANALYSIS

In this guideline, the Detailed Flow Measurement Techniques Committee has outlined a pragmatic approach that considers the overall uncertainty level of a PIV measurement in a realistic test environment. The proposed approach needs to be fully implemented and evaluated in a rigorous fashion.

7. REFERENCES

Adrian, R.J., Yao, C.S., 1985, "Pulsed laser technique application to liquid and gaseous flows and the scattering power of seed materials," Appl. Optics, vol. 24, pp. 44–52.

Harrison, E.L., Atsavapranee, P., 2014, "Optics optimization calculations for particle image velocimetry (PIV) torpedo design: Scheimpflug mechanism," Naval Surface Warfare Center Carderock Division Hydromechanics Directorate Technical Report, NSWCCD-80-TR-2014/xxx.

Keane, R.D., Adrian, R.J., 1990, "Optimization of particle image velocimeters. Part I: Double pulsed systems," Meas. Sci Technol., vol. 1, pp. 1202–1215.

Keane, R.D., Adrian, R.J., 1991, "Optimization of particle image velocimeters. Part II: Multiple pulsed systems," Meas. Sci Technol., vol. 2, pp. 963–974.

Keane, R.D., Adrian, R.J., 1992, "Theory of cross-correlation analysis of PIV images," Applied Scientific Research, vol. 49, pp. 191–215.

Lawson, N. and Wu, J., 1997a, "Three-dimensional particle image velocimetry: error analysis of stereoscopic techniques," Meas. Sci Technol., vol. 8, pp. 894–900.

Lawson, N. and Wu, J., 1997b, "Three-dimensional particle image velocimetry: experimental error analysis of a digital angular stereoscopic system," Meas. Sci Technol., vol. 8, pp.1455–1464

Prasad A.K. and Jensen K., 1995, "Scheimpflug stereocamera for particle image velocimetry in liquid flows", Appl. Optics, Vol. 34, No. 30, pp. 7092–7099.

Prasad A.K., Adrian R.J., Landreth C.C., Offutt P.W., 1992, "Effect of resolution on the speed and accuracy of particle image velocimetry interrogation", Experiments in Fluids, Vol. 13, pp. 105–116.

Raffel, M., Willert, C., Kompenhans, J., 1998, "Particle Image Velocimetry," Springer ISBN 3-540-63683-8.

Stanislas, M., Okamoto, K. and Kähler, C., 2003, "Main results of the First International PIV Challenge," Meas. Sci Technol., vol. 14, pp. R63–R89.

Stanislas, M., Okamoto, K., Kähler, C. and Westerweel, J., 2005, "Main results of the Second International PIV Challenge," Exp. Fluids, vol. 39, pp. 170–191.

Stanislas, M., Okamoto, K., Kähler, C., Westerweel, J. and Scarano, F., 2008, "Main results of the Third International PIV Challenge," Exp. Fluids, vol. 45, pp. 27–71.

van Doorne, C.W.H. and Westerweel, J., 2007, "Measurement of laminar, transitional and turbulent pipe flow using Stereoscopic-PIV," Exp. Fluids, vol. 42, pp. 213–227.

Westerweel, J., Dabiri, D., and Gharib, M., 1997, "The effect of a discrete window offset on the accuracy of cross-correlation analysis of PIV recordings," Exp. Fluids, vol. 23, pp. 20–28.

Willert, C., 1996, "The fully digital evaluation of photographic PIV recordings," Appl. Sci. Res., vol. 56, pp. 79–102.

8. APPENDIX A: A SIMPLE MODEL FOR AN SPIV IMAGING SYSTEM

Geometrical description of an SPIV camera with a Scheimpflug mechanism

Consider the optical configuration presented in Figure 3, which is a representation of the imaging system of one camera in an SPIV setup. A lens images an object plane (light sheet) at an oblique angle, with the lens axis intersecting the origin of the field of view (FOV) at an angle θ. The distance along the lens axis to the origin of the FOV, or the nominal object distance, is d_o. The imaging system utilizes a Scheimpflug mechanism that allows the lens to be shifted and tilted relative to the image plane. Since the object plane is at an oblique angle to the lens, the ability to shift and tilt the lens allows the object plane to be optimally focused onto the sensor array. This optical arrangement is called the Scheimpflug condition, whereby the object plane, the lens plane, and the image plane are collinear as illustrated in Figure 3.

In order to describe the projection of a point on the object plane onto a point on the CCD, we define three coordinate systems: the object plane coordinate system (X, Y, Z), the CCD coordinate system (x, y, z), and a coordinate system native to the imaging lens (χ, υ, ζ). For simplicity, we pick point A in the object plane with the coordinate $(0, Y_A, 0)$ and will now describe how to project this point onto the CCD.
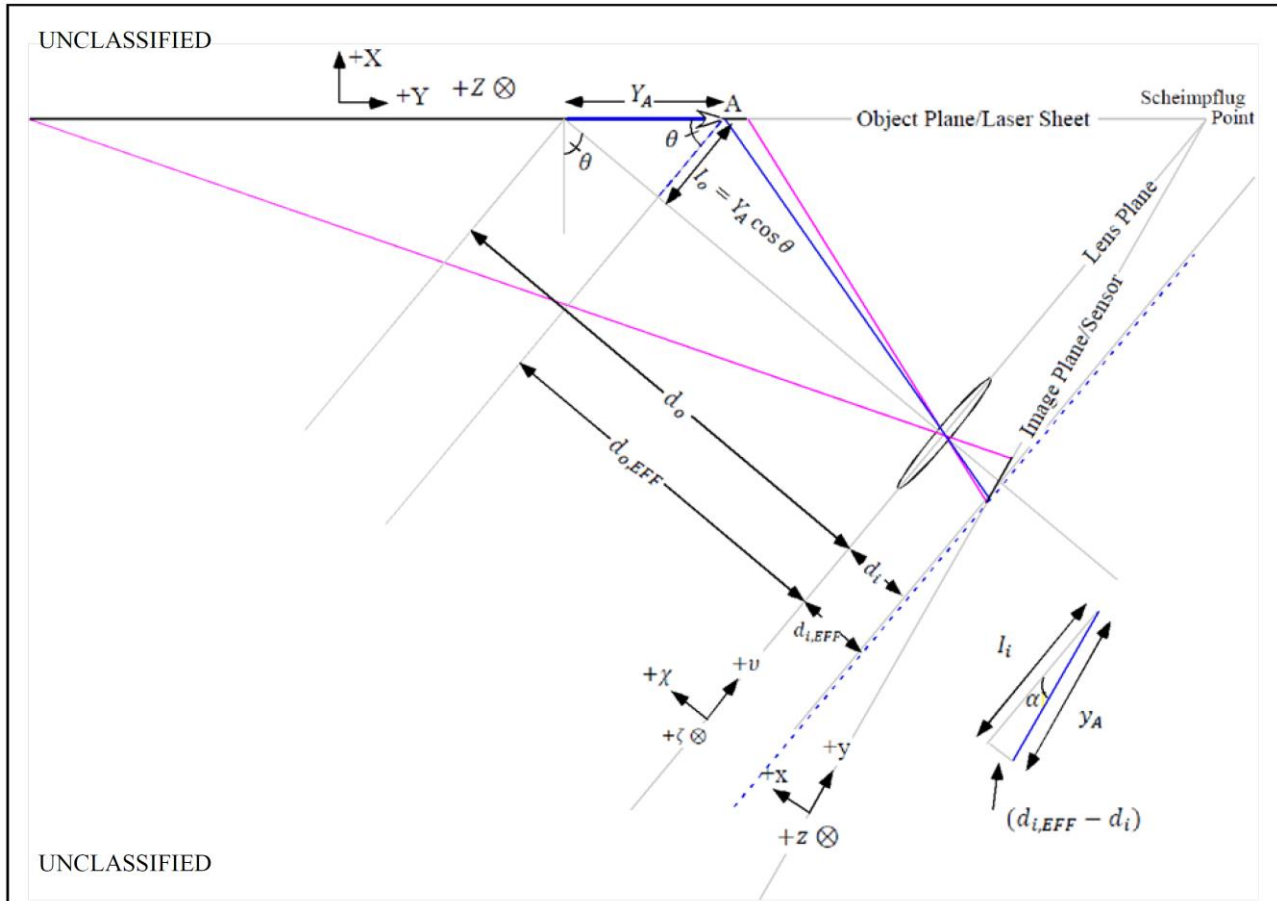
Figure 3: Schematic of an SPIV imaging configuration satisfying the Scheimpflug condition

In the lens coordinate system, we can apply the thin lens equation:

$$\frac{1}{d_o} + \frac{1}{d_i} = \frac{1}{f} \, . \tag{11}$$

Therefore, the distance from the lens center to the origin of the CCD, or the nominal image distance, is simply:

$$d_i = \frac{1}{\left(\frac{1}{f} - \frac{1}{d_o}\right)} \, . \tag{12}$$

Upon inspection of the diagram in Figure 3, point A is at an object distance,

$$d_{o,EFF} = d_o - Y_A \sin\theta \, , \tag{13}$$

in the lens coordinate system, with an object height,

$$I_o = Y_A \cos\theta. \tag{14}$$

Using the thin lens equation, we can write the image distance and image height in the lens coordinate system as Equations (15) and (16),

$$d_{i,EFF} = \frac{1}{\frac{1}{f} - \frac{1}{d_{o,EFF}}} \tag{15}$$

$$I_i = \frac{d_{i,EFF}}{d_{o,EFF}} I_o \tag{16}$$

In the CCD coordinate system, point A is projected onto the CCD at $(0, y_A, 0)$, where the distance y_A is given by Equation (17).
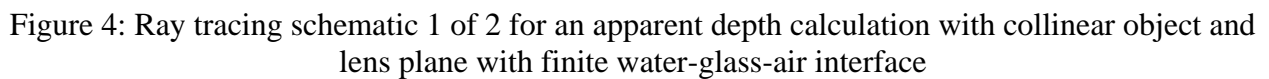
$$y_A = -sgn(Y_A)\sqrt{\left(d_{i,EFF} - d_i\right)^2 + I_i^2} \tag{17}$$

Modelling the index of refraction step changes in underwater applications

In actual underwater applications, the SPIV optical setup is further complicated by the index of refraction step changes, caused by the placement of the camera inside an underwater housing for tow tank applications or the placement of the camera in air looking through the optical window of a cavitation tunnel. For cavitation tunnel applications, a recommended practice is the use of a "water prism," so that the lens is imaged through an air/glass/water interfaces which are parallel to the lens axis.

Harrison & Atsavapranee (2014) describes the full mathematical model of this complex optical setup within the framework of the thin-lens assumption. Figure 4 and 5 show detailed schematics where:

- the object plane and lens plane are collinear
- a water-glass-air interface has a finite thickness, T, and
- the refractive interface is parallel to the lens place but not to the object plane

Figure 4: Ray tracing schematic 1 of 2 for an apparent depth calculation with collinear object and lens plane with finite water-glass-air interface
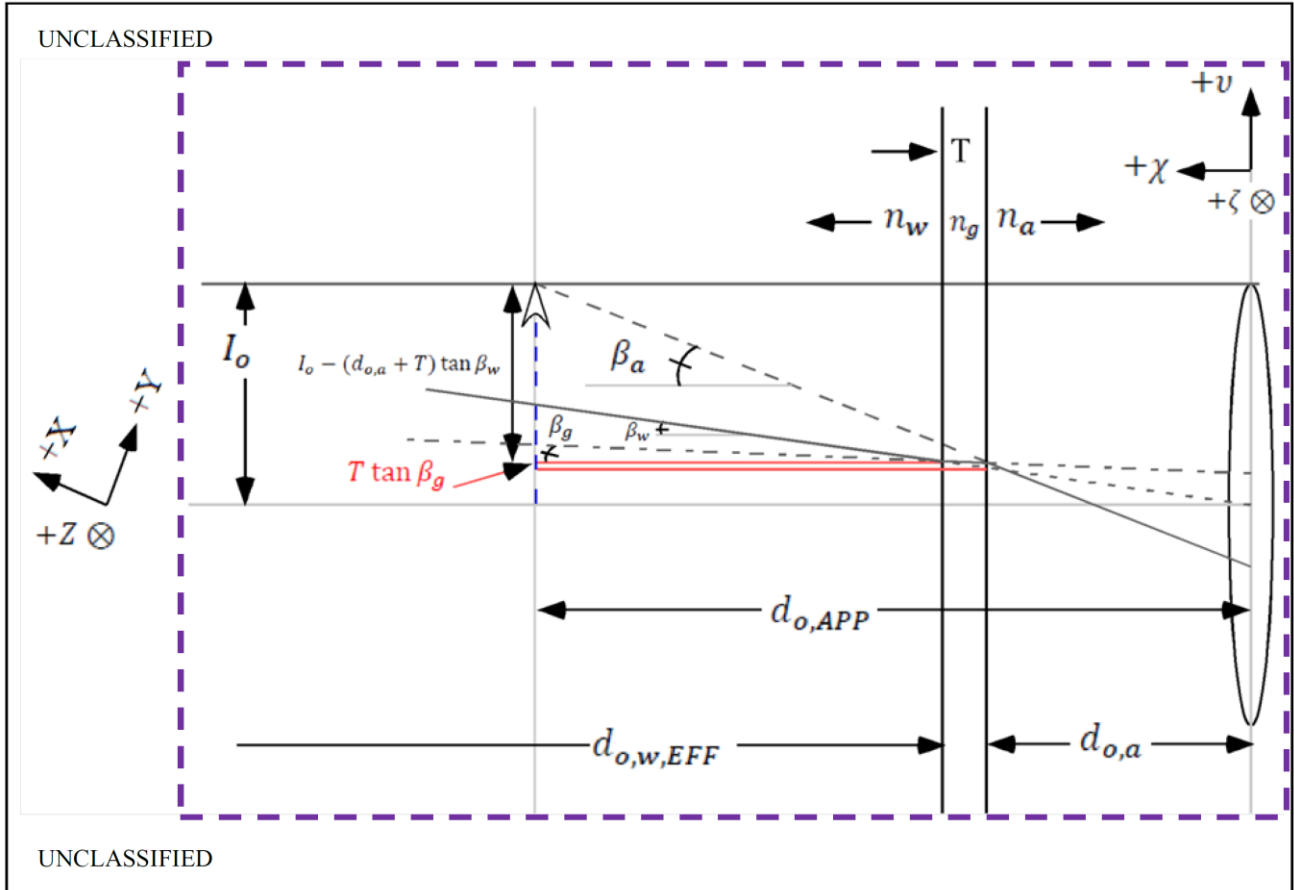
Figure 5: Ray tracing schematic 2 of 2 for an apparent depth calculation with collinear object and lens plane with finite water-glass-air interface

The presence of the refractive interfaces can be described as causing the object to appear closer than the actual object distance. In other words, the object would appear to be at an apparent object distance, $d_{o,APP}$. Equations (18) and (19) are determined by inspection of Figures (4) and (5).

$$I_o = Y_o cos\theta \qquad (18)$$

$$d_{o,ANG} = Y_o sin\theta \qquad (19)$$

$$d_{o,w,EFF} = d_{o,w} - d_{o,ANG} \qquad (20)$$

$$d_{o,EFF} = d_{o,w,EFF} + d_{o,a} + T \qquad (21)$$

The location of the apparent object is defined by Equations (22)-(25).

$$tan\beta_w = \frac{I_o}{d_{o,EFF}} \qquad (22)$$

$$sin\beta_g = \frac{n_w}{n_g} sin\beta_w \qquad (23)$$

$$sin\beta_a = \frac{n_g}{n_a} sin\beta_g = \frac{n_w}{n_a} sin\beta_w \qquad (24)$$

$$d_{o,APP} = d_{o,a} + \frac{I_o - (d_{o,a}+T)tan\beta_w + T tan\beta_g}{tan\beta_a} \qquad (25)$$

Therefore, if the camera in Figure 3 is placed in an underwater housing and the experiment is performed underwater, Equations (15) and (16) become:

$$d_{i,EFF} = \frac{1}{\frac{1}{f} - \frac{1}{d_{o,APP}}} \qquad (26)$$

$$I_i = \frac{d_{i,EFF}}{d_{o,APP}} I_o \qquad (27)$$